Surface relaxation in protein crystals

S. Boutet,[1] I. K. Robinson,[1] Z. W. Hu,[2] B. R. Thomas,[2] and A. A. Chernov[2]

[1]*Department of Physics, University of Illinois, Urbana, Illinois 61801*
[2]*Universities Space Research Association, Marshall Space Flight Center, Huntsville, Alabama 35875*

Surface x-ray diffraction measurements were performed on (111) growth faces of crystals of the cellular iron-storage protein, horse spleen ferritin. Crystal truncation rods (CTR) were measured. A fit of the measured profile of the CTR revealed a surface roughness of 48 ± 4.5 Å and a top layer spacing contraction of $3.9 \pm 1.5\%$. In addition to the peak from the CTR, the rocking curves of the crystals displayed unexpected extra peaks. Multiple scattering is demonstrated to account for them. Future applications of the method could allow the exploration of hydration effects on the growth of protein crystals.

I. INTRODUCTION

Knowledge of the atomic structures of biological macromolecules, especially proteins, is an essential prerequisite to understanding their function [1]. A powerful way to obtain the structure is to use x-ray diffraction on artificial crystals, usually obtained by gently precipitating the molecule from solution. So far, about 15 000 structures deciphered to various accuracies are stored in protein data banks. Some protein crystals, such as insulin and lysozyme, are produced by the pharmaceutical industry and require control of their polymorph modification, purity, and habit. However, in at least 50% of cases, trial-and-error screening and optimization, now employed to find the composition of the solution resulting in crystallization, do not allow to obtain high quality crystals or crystallization at all. The search for the right crystal modification and properties for applications also remains empirical. Biomacromolecular crystallization remains an art rather than science. Growing crystals of high perfection remains a bottleneck in structural biology and limits capabilities to grow crystals for some other purposes.

The perfection of a biomacromolecular crystal is the most important issue since it determines the structural resolution of atomic positions within the molecule. There are numerous proteins for which the known crystallization conditions result in small (~ 100–300 μm or less) crystals diffracting to 4 Å or more, which is insufficient for atomic resolution. Application of modern synchrotron radiation techniques [2,3] makes it possible to obtain diffraction patterns from crystals as small as 50–100 μm, but even this is sometimes impossible. These are motivations to study the physical properties of biomacromolecular crystals and their surfaces, since processes on these surfaces determine crystal perfection and growth kinetics [4].

Biomacromolecular crystals form a large class of solids within which the size of building units, the macromolecules, exceeds the range of intermolecular forces by orders of magnitude [5]. For instance, the apoferritin molecules are spheres of 130 Å diameter. Unlike colloidal crystals, however, the intermolecular binding in protein crystals is very specific. The violation of this specificity during crystallization may lead to optically isotropic and well faceted crystals with rotational disorder, which diffract x rays very poorly. Biomacromolecular crystals are one to two orders of magnitude more compressible than conventional solids. Because of their wide variety of potential contacts, biomolecules can attain multiple configurations at their surfaces. In some cases this can impede growth. These specific features makes biocrystalline surfaces fundamentally interesting.

Biomacromolecular crystals follow the same general crystallization laws as the crystals of small molecules, with essential corrections for the specific features mentioned above. Biocrystals are typically faceted suggesting that the facets are smooth on the molecular scale. In other words, the steps on these facets have free energies per molecular site exceeding thermal energy and the wide terraces between the steps are well ordered. Therefore, the biocrystals grow layer by layer, by step propagation, with the new layers generated either by two-dimensional nucleation or by screw dislocations. This surface morphology and growth kinetics was extensively addressed by interferometry and atomic force microscopy (AFM) [6–10]. In particular, it was found that on the (111) face of ferritin crystals new layers are exclusively generated by two-dimensional nucleation rather than by dislocations [11,12].

Reconstruction of the (010) face of orthorhombic lysozyme crystals has been observed by atomic force microscopy: the lattice period along the a axis was found to be doubled by surface corrugation [13]. Image processing of the steps on the prismatic face of tetragonal lysozyme also revealed period doubling [14]. However, to the best of our knowledge, no x-ray diffraction studies of the surfaces of the macromolecular crystals have been published so far. With these incentives, we applied x-ray diffraction to analyze the (111) face of a model crystal, horse spleen ferritin. Surface diffraction has proven in the past to be an extremely useful tool in studying the surfaces of inorganic crystals and could represent an interesting technique for the study of protein crystal growth. Surface x-ray diffraction has the advantage of probing many layers of the surface to get 3D information rather than being explicitly surface-sensitive like AFM. This

allows the study of the phenomenon of surface relaxation, and hence the response to the intermolecular forces at the surface.

II. MATERIALS AND SAMPLE PREPARATION

Ferritin has the physiological function of storing iron atoms until they are needed by the body. The ferritin molecule is a quite large spherical shell molecule (inner diameter ~ 80 Å and outer diameter ~ 130 Å and mass$=450\,000$ Da) which crystallizes in the face centered cubic (fcc) lattice with lattice parameter $a = 184$ Å. Horse spleen ferritin (Sigma Co.) was purified from higher molecular weight oligomers (dimer, trimer, etc.) and other impurities with a fast protein liquid chromatography apparatus including a Superdex Hi Load 200, 26/60 gel filtration column (Amersham Biosciences, Piscataway, NJ) in $0.2M$ sodium acetate buffer pH 5.0 [15,16]. The process of ferritin purification to microhomogeneity has resulted in the improvement in the x-ray diffraction resolution from 2.6 to 1.8 Å [15]. Approximately 100 crystals were formed in a diffusion controlled crystallization apparatus for microgravity (DCAM) with an increasing gradient of cadmium sulfate in $0.2M$ sodium acetate pH 5.0 over a period of 1 month [17]. Crystals were transferred from the DCAM apparatus to x-ray capillaries for analysis in the crystallization buffer. One of the reasons why it was chosen to look at holoferritin (the iron-containing version of the ferritin molecule) is the fact that the interior of each shell is filled with up to 4500 atoms of iron in ferrihydrite form. Reference [18] gives a full review of the ferritin structure and biological functions. This iron core scatters the x rays very strongly producing a large signal to be detected, at least for small-angle reflections. Another reason why we chose to work with ferritin is the fact that it crystallizes in a simple crystal form, which simplifies the analysis.

The quartz capillary containing the crystal was mounted vertically on the Kappa diffractometer at the X16C beam line at the National Synchrotron Light Source (NSLS) on the Brookhaven National Laboratory site. This diffractometer has the advantage of manual setting of the angles and high speed due to its direct-drive servo motors [19]. The crystal faces studied were the growth faces which are the {111} crystal faces. The crystals had nice octahedral morphologies and large sizes ($\sim 1 \times 1 \times 1$ mm^3), which allowed the visual alignment of one of the faces into the beam. This allowed us to manually line up the desired crystal face parallel to the incoming x-ray beam in order to rapidly locate the corresponding (111) Bragg peak. The beam was focused to a size of 200 μm horizontally and 1.5 mm vertically using a saggitally focused Si(111) double-crystal monochromator, which also selected a single wavelength from the white beam produced by the source. The beam was then cut to 200 $\times 200$ μm^2 with slits. The data collecting software (SUPER) used allowed us to perform the desired scans quickly before radiation damage from the strong synchrotron beam became too extensive.

In order to understand the significance of the scans performed, we first need to briefly discuss surface x-ray diffraction and crystal truncation rods.

III. CRYSTAL TRUNCATION RODS

The high brilliance of a synchrotron source is important for surface x-ray experiments, since scattering from surfaces is weak. The x-ray beam produced from a synchrotron source such as the NSLS can be accurately approximated as a sum of plane waves. The use of a monochromator upstream of the sample filters out all the wavelengths except for a very narrow range near a desired value. Thus, to a very good approximation, we take the incoming beam as a monochromatic plane wave with wave vector $\mathbf{k}$. This wave impinges on the surface of a crystal. Due to the large penetration depth of x rays, many layers of the crystals are penetrated, and diffraction from the bulk of the crystal is observed along with diffraction from the surface. In fact, due to this large penetration, most of the diffraction comes from bulk scattering and only a small signal comes from the surface. We treat the diffraction of the plane wave in the far field limit as we place the detector far away from the sample.

We will assume for now a perfect infinite crystal. In the kinematical approximation, the presence of the bulk crystal produces a scattered plane wave with wave vector $\mathbf{k}'$ with intensity given by [20]

$$I \propto \lim_{N_1,N_2,N_3 \to \infty} |F_{cell}|^2 \frac{\sin^2\left(\frac{1}{2}N_1 q_1 a_1\right)}{\sin^2\left(\frac{1}{2}q_1 a_1\right)}$$
$$\times \frac{\sin^2\left(\frac{1}{2}N_2 q_2 a_2\right)}{\sin^2\left(\frac{1}{2}q_2 a_2\right)} \frac{\sin^2\left(\frac{1}{2}N_3 q_3 a_3\right)}{\sin^2\left(\frac{1}{2}q_3 a_3\right)}, \quad (1)$$

where F_{cell} is the structure factor of the unit cell of the crystal, $q_i = k_i' - k_i$, a_i, and N_i are, respectively, the components of the momentum transfer, the lattice parameter, and the number of unit cells in the ith direction. Taking the limit yields δ functions at the Bragg peaks when the Laue conditions are satisfied: $q_1 a_1 = 2\pi H$, $q_2 a_2 = 2\pi K$, and $q_3 a_3 = 2\pi L$, where H,K,L are the integer Miller indices [21].

We now look at a truncated crystal; that is, a crystal which is infinite in both x_1 and x_2 directions (the directions parallel to the surface) and semi-infinite in the x_3 direction (perpendicular to the surface) instead of looking at an infinite crystal as above. This introduces a surface which makes the sum over N_3 no longer infinite. The effect is that the intensity is no longer concentrated in δ functions in the q_3 direction. Then, measurements where there would be no intensity in the case of infinite crystals (at $q_3 \neq 2\pi L/a_3$) can yield information about the surface. When this condition on q_3 is relaxed, the intensity observed is given by, when $q_1 a_1 = 2\pi H$ and $q_2 a_2 = 2\pi K$ [20],

$$I \propto \lim_{N_1, N_2 \to \infty} |F_{cell}|^2 \frac{\sin^2\left(\frac{1}{2}N_1 q_1 a_1\right)}{\sin^2\left(\frac{1}{2}q_1 a_1\right)}$$

$$\times \frac{\sin^2\left(\frac{1}{2}N_2 q_2 a_2\right)}{\sin^2\left(\frac{1}{2}q_2 a_2\right)} \frac{1}{2\sin^2\left(\frac{1}{2}q_3 a_3\right)}$$

$$= N_1^2 N_2^2 \frac{1}{\sin^2\left(\frac{1}{2}q_3 a_3\right)}. \tag{2}$$

The key point of this equation is that the diffraction coming from the surface for a certain value of q_3 is repeated at every value of q_1 and q_2 that fulfills the Bragg condition. The intensity is close to zero for all values of q_1 and q_2 except for those satisfying the first two Laue conditions, i.e., there is diffracted intensity only near Bragg peaks from the bulk. This scattered intensity from the surface, contrarily to the scattered intensity from the bulk, is not limited to points in reciprocal space. The relaxation of the third Laue condition means that the intensity in the direction perpendicular to the surface is spread out. What is obtained are continuous streaks of intensity or Bragg rods in the q_3 direction, connecting all the bulk Bragg points. These lines are called crystal truncation rods (CTR's).

In the real world, crystals are not infinite in any direction. Furthermore, the x-ray beam does not illuminate an infinite volume. The Bragg peaks are then no longer δ functions, but extend in all directions. This spread is inversely proportional to the volume illuminated by the beam or the volume of individual crystal grains. The resolution of the apparatus will often broaden the peaks further. One can distinguish diffraction from the surface from simple mosaic broadening of the bulk peaks or even crystal size effects using the fact that truncation rods are extended in only one direction (perpendicular to the surface), while other effects broaden the peaks in all directions. Only the presence of a surface gives rise to streaks of intensity.

Another factor to include in the calculation of the CTR profile is the surface roughness. The surface will likely not be flat at the molecular level and will rather contain terraces, vacancies, or steps. The presence of extra molecules or the absence of some in the surface will cause interference with the diffracted wave from the bulk and this will cause a reduction in the intensity of the truncation rod by a factor depending on the height statistics of the surface. The changes in height of a rough surface mean that the different parts of it scatter the x rays with a different phase causing destructive interference. Thus, surface roughness can be measured with x rays as long as the excursions in height are smaller than the longitudinal coherence length of the beam, i.e., as long as the phase of the beam is well defined over all the layers making up the surface. Using a Si monochromator, the longitudinal coherence length is of order 1 μm, making it possible to measure the roughness over many layers of ferritin crystals. Many models for the surface roughness and their corresponding scattered intensities have been studied and can be found in the literature [20,22].

Proteins crystals do not diffract as strongly as inorganic crystals, resulting in a fairly low intensity of the CTR's. Also, proteins are very sensitive to radiation and the strong x-ray beam from the synchrotron caused a lot of radiation damage over a very short period of time. The peaks measured were observed to significantly weaken and even disappear on the scale of 30 min of irradiation. This means that only a few points along the rods could be measured in the time before the damage became too extensive. Combined, the low intensities from the CTR's measured, as well as the small number of q_3 values sampled made the determination of a value for the roughness inaccurate. Nevertheless, a simple model could be used to get an estimate of the roughness. The CTR's are also sensitive to the surface relaxation, that is, whether the surface spacing is contracted or dilated. The top layer, having uncompensated bonds due to the missing layer above it, will generally not find its equilibrium position to be the same as that of the bulk layers. In the case of proteins, this is the object of our study as it can relate to hydration effects. The missing bonds will cause the top layer to move either up or down depending on the energetics of the system, a phenomenon known as relaxation. This has the effect of changing the value of the perpendicular lattice vector which shifts the whole intensity profile of the CTR in q space either toward larger q_3 for contraction or smaller q_3 for dilation [20]. This relaxation can in some crystals propagate many layers down and cause other layers near the top to move from their bulk positions. The question of whether a protein crystal has a dilated or contracted surface is not known for any example.

IV. RESULTS

As mentioned above, the diffraction from the surface can be observed near any bulk Bragg peak accessible with the experimental setup. In the present case, the very low intensity and short specimen lifetime made it difficult to observe any surface diffraction at all. We therefore restricted our studies to the specular CTR, i.e., the (111) rod, measuring only around the (111) Bragg peak, which was very easy to align. The crystals where kept hydrated in the mother liquor inside a quartz capillary of 1 mm diameter. A large amount of water was then illuminated by the beam. This gave rise to a large background radiation and it was necessary to observe a CTR by performing a scan which cuts through it in reciprocal space. For the specular CTR, a rocking scan (ω scan) does the job. Such a scan allows to vary $q_\parallel$, parallel to the studied surface, while keeping q constant as shown in Fig. 1. Hence, by rocking the crystal about the specular direction and keeping the detector fixed, we expect to see a peak in the middle of the scan which represents the CTR. Such scans are shown as a function of the orientation ω in Fig. 2. The series of scans shown are for various values of $H = K = L$, that is, at various heights along the rod in reciprocal space, both above and below the bulk Bragg peak. As the scans move further
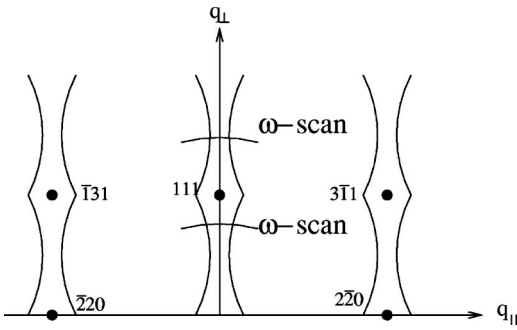
FIG. 1. The reciprocal space of a fcc crystal truncated at a (111) face. The streaks extending between the Bragg peaks are the crystal truncation rods. The lines cutting the (111) rod represent the rocking scans (ω scans) performed both above and below the Bragg peak.

away from the bulk peak, the maximum in intensity observed in the middle of the scan diminishes. This is expected from the $1/\sin^2(q_3 a_3/2)$ dependence of the intensity away from the Bragg peaks. We found, unexpectedly, the presence of two more peaks on some of the scans. Close inspection of the data reveals the following. One of the extra peaks always appears at $\omega = \omega_{Bragg}$, or when the Bragg condition on the incoming beam is satisfied as shown in Fig. 3(a). As for the second extra peak, as shown in Fig. 3(b), it always appears at the same value of $2\theta - \omega = \omega_{Bragg}$, where 2θ is the scattering angle. A simple geometrical explanation of this phenomena is shown in Fig. 4.

Let us consider a scan corresponding to a value of q_3 or $q_\perp$ below the Bragg peak. This requires that the detector is set at an angle smaller than the 2θ angle of the Bragg reflection. The slits were set narrow enough that the bulk Bragg peaks could never be reached for any setting of the crystal during the rocking scans. The solid lines show the beam satisfying the Bragg condition. Picture (a) displays how the
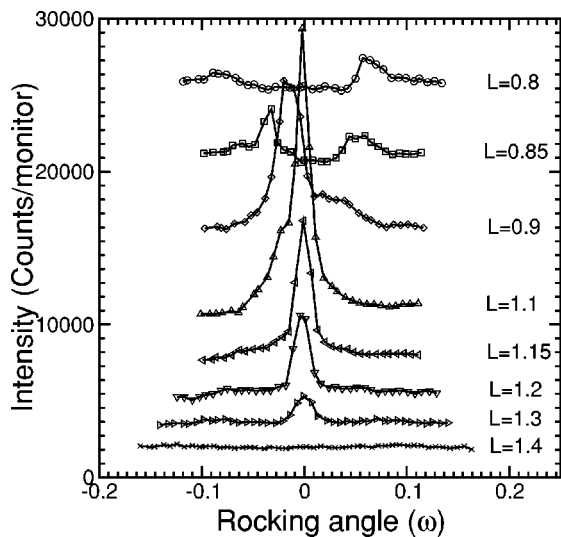
FIG. 2. Series of rocking scans of a ferritin crystal at different values of $H = K = L$ above and below the Bragg peak. Three peaks can be seen in some of the scans. The central peak is identified as the CTR.
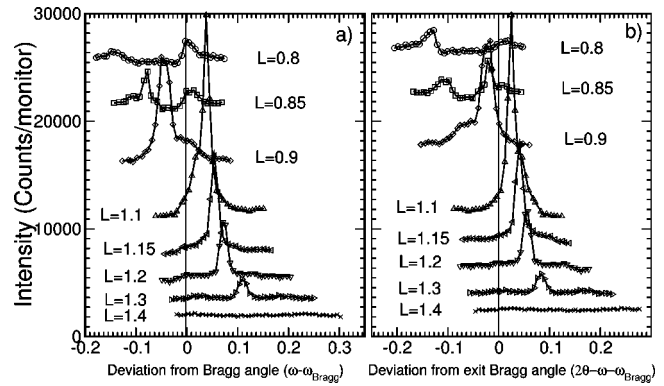
FIG. 3. (a) Same rocking scans as shown in Fig. 2 with the data now plotted versus $\omega - \omega_{Bragg}$. We see that one of the two extra peaks occurs when $\omega - \omega_{Bragg} = 0$, i.e., when the incident beam meets the Bragg condition for the 111 reflection. (b) Same rocking scans as (a) with the intensities now plotted versus $2\theta - \omega - \omega_{Bragg}$, or the exit angle. Notice that the third peak in the scans now occurs at $2\theta - \omega - \omega_{Bragg} = 0$.

peak at $\omega = \omega_{Bragg}$ arises. The incoming beam impinges on the surface at the angle satisfying the Bragg condition for specular reflection. This gives rise to a very strong Bragg diffracted beam reflected at the same angle ω_{Bragg}, which misses the detector due to the presence of collimating slits. This intense beam can scatter from the water molecules present inside the quartz capillary or inside the crystal itself. A few of the x rays after being Bragg reflected are thus scattered into the detector. As the angle ω is varied away from the ω_B value, there no longer exists an intense reflected beam to be small-angle scattered into the detector, and the
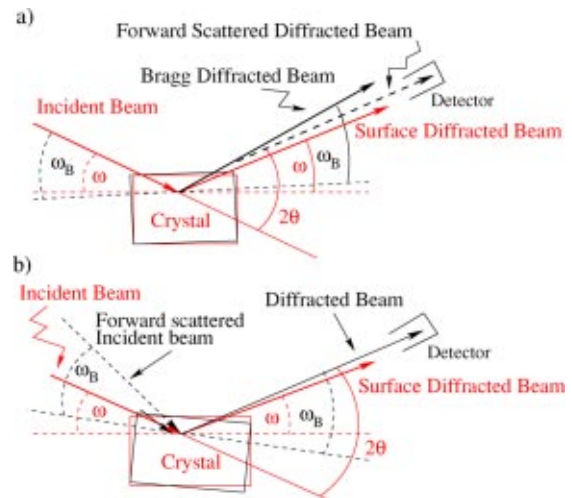
FIG. 4. Diagram showing the geometry of the incident and exit beams showing how three peaks can arise from the rocking scans. (a) The incident beam gives rise to an intense reflected beam as the Bragg condition is met. This large Bragg reflected beam (solid line) is then scattered by the water and the air molecules into the detector (dashed line). (b) The incident beam (solid line) is scattered by the water and air molecules into the Bragg condition (dashed line). A sizable fraction of the x rays thus scattered are then reflected into the detector since they satisfy the Bragg condition.

measured intensity goes down. Figure 4(b) shows how the reverse situation can give rise to the second extra peak. This time, the Bragg condition is satisfied for the *reflected* beam instead of the incident beam. The intense incident beam (solid line) is small-angle scattered by the air, water, or in-homogeneities in the crystal and some of those scattered x rays happen to be scattered just right into the Bragg condition (dashed line). Those x rays thus scattered get Bragg reflected by the crystal into the detector, giving rise to a peak at a value of $2\theta - \omega = \omega_B$. This peak gets larger as we come nearer the value $L = 1$. This is because as the Bragg condition is approached, the additional scattering angle gets smaller and the number of x rays scattered increases since small-angle x-ray scattering is stronger at smaller angles.

The situation is similar for scans above the Bragg peak. The pictures shown predict that the closer the performed rocking scans are to the bulk Bragg peak, the closer the two extra peaks are to the CTR peak, until a certain point when they become indistinguishable from the CTR and even the Bragg peak itself. After crossing the Bragg peak, the two extra peaks cross over and move apart again. This can be seen in Fig. 3. As the value of $H = K = L$ gets close to 1, the peaks grow closer and eventually merge. This mechanism should apply, in general, whenever CTR's are measured, but the effect is much stronger for protein crystals because of the large quantity of solvent illuminated by the beam (which scatters a lot) and because of the small diffraction angles involved with large unit cells as in protein crystals. The effect is large enough so that the extra peaks can be larger than the CTR itself.

Having explained the presence of the two extra peaks, we can disregard them and integrate the intensities of only the central peaks of each rocking scan. These integrated intensities were extracted and plotted versus q_3 in Fig. 5. An asymmetry between the two sides of the Bragg peak can be seen, which would not be present in the case of a perfect surface [see Eq. (2)]. A fit to the data was performed allowing for vertical displacements of the top layer. The interference between this layer and the bulk gives rise to the asymmetry observed. The small number of data points did not allow us to use an elaborate model to estimate the surface roughness. Only an occupation ratio of the top layer was allowed to vary, along with the position of the top layer and a scale factor. The three parameter fit to the data is shown in Fig. 5 and yielded a $3.9 \pm 1.5\%$ contraction of the top layer, corresponding to a displacement of 4.1 Å as well as an occupation ratio of 72%. With only 72% of the top layer occupied, the other 28% of the surface has the layer below exposed, making this second layer effectively the top crystal layer for 28% of the surface area. This layer, since exposed to the solvent, is also expected to relax and the fit allowed for a relaxation identical to the very top layer. Combining the occupation ratios and the contraction of the top two crystal layers, one can readily calculate the rms surface roughness σ_{rms}, which is the square root of the average of the height variation over the length scale of the lateral coherence of the beam. For the beam used, the lateral coherence is of order 1000 Å. This means that fluctuations in the height of the surface separated by distances larger than 1000 Å in the plane of the surface
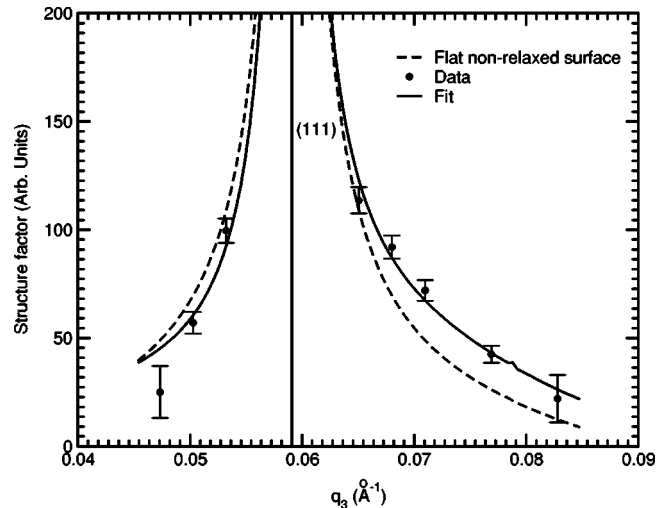
FIG. 5. Truncation rod profile around the (111) Bragg peak. The data are shown with error bars and the solid line is the fit obtained by letting the top layer be free to move up or down, as well as having only partial occupation of the lattice sites. The fit yields a 3.9% contraction along with an rms roughness of $\sigma_{rms} \approx 48$ Å. The dashed line represents the rod profile with no relaxation of the top crystal layer.

are not resolved. Our data cannot then rule out the presence of a few large steps separated on average by a few tenths of a micron. The model implied is shown in Fig. 6. The roughness was calculated by averaging over the two surface layers used in the fitting model and we found $\sigma_{rms} = 48 \pm 4.5$ Å, which corresponds to close to half a crystal layer.

The contraction of the top layer causes the rod to be more intense on the high side of the Bragg peak. Such a relaxation is to be expected due to the presence of uncompensated bonds in the top layer of the crystal. However, depending on the energetics of the system, this could also lead to a dilation instead of a contraction, for example. So the presence of relaxation is no surprise, but its direction and magnitude constitute an interesting result.

V. DISCUSSION

Having shown that crystal truncation rods from protein crystals can be measured, it would now be interesting to push this investigation further. The field of inorganic surface x-ray diffraction has yielded over the years many important results about surface structure and growth mechanism. It is hoped that the same can be true for protein crystals, and that *in situ* studies of the growth of such protein crystals can be performed under different growth conditions, possibly yielding new insights into the growth mechanisms.

One can easily speculate about the possible applications of surface x-ray diffraction for the study of protein crystal growth. For example, the effects of slight dehydration on the in-plane structure of the surface could be measured as a function of solvent composition. One could also see the effects of poisoning of the surface by impurities and learn more about the importance of impurities in protein crystal growth.
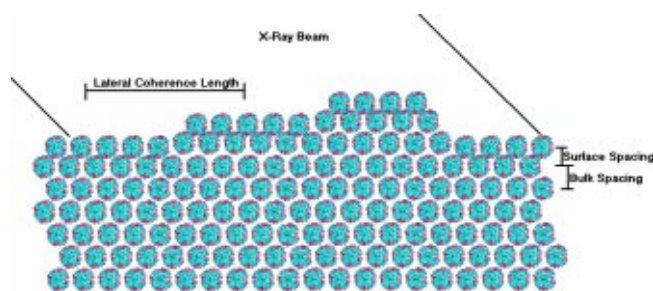
FIG. 6. Model of the crystal surface used to fit the CTR profile. The layer exposed to the solvent relaxes inward by 3.9%. The partial occupancy of the very top layer means that the second layer is sometimes exposed and relaxes. Fluctuations in the height of the surface separated by distances larger than the coherence length cannot be ruled out and are shown here as a large step.

A less easily realized possibility would be to study the growth by looking at a nucleation layer on some suitable substrate, perhaps templated to match the spacing of the protein crystal. This could be easily visualized, but as for most protein crystal x-ray studies, the limitations do not come from the experimental techniques but rather from the sample preparation and lifetime. It might prove difficult to find a suitable substrate for such a study. However, if one could produce a sample grown on a fixed substrate, many of the problems of the technique could be reduced significantly. For example, alignment would be readily achieved, but most important of all, the signal could be greatly increased with a large surface and the absence of bulk diffraction. Valuable information could be obtained about the growth mechanisms.

The $\sim 4\%$ relaxation is a figure within the typical range for inorganic materials, for example, metals in vacuum [23]. For ionic crystals, the relaxation is usually weaker though less data is available. For conventional molecular crystals, the effect is even less studied, but is not supposed to be strong due to weaker intermolecular interactions. Thus, at first glance, the 3.9% relaxation of the first (111) surface plane of ferritin is not a big surprise. However, it is actually not trivial because biomacromolecules are much harder than the crystals built of these molecules, and the size of macromolecules strongly exceeds the range where intermolecular forces are effective. Indeed, the isothermal compressibility of eight proteins in solution has been studied. The bulk elastic modulus of these molecules was found to vary within the range (30 ± 7) GPa $= (3 \pm 0.7) \times 10^{11}$ dyn/cm^2 [24]. If instead the protein molecule is considered to be a solid material, we can describe it by the Young modulus $E = 3K(1 - 2\nu)$, where K is the bulk modulus. With the Poisson ratio assumed to be $\nu = 0.25$, that means $E = \sim 1.5K$. On the other hand, measurements of the Young moduli from the resonance vibration frequency of a crystalline protein rod for cross-linked lysozyme, hemoglobin, and myoglobin provided E

$=1$, 0.5, and 0.4 GPa, respectively [25,26]. Three point bending measurements for non-cross-linked lysozyme crystals in solution resulted in $E = 0.1$–0.5 GPa [27]. The crystal is more than ten times less hard than the molecules it is made of. An intermolecular contact covers only a small fraction of the surface of a molecule and so has a much lower hydrogen bond density within the intermolecular contact.

The diameter of spherical ferritin molecule is 130 Å, which means the lattice spacing in the (111) direction is 106 Å. Thus, the 3.9% relaxation is equivalent to the absolute contraction of the distance between the center of a molecule in the top molecular plane and its neighbor in the second plane by 4.1 Å. The hydrogen bond length (in ice) is 1.76 Å [28] and, at atmospheric pressure, a similar figure may be expected for the hydrogen bonds, which make major contributions to the intermolecular contacts in protein crystals (along with van der Waals forces). It seems clear that the 4.1-Å compression cannot be accommodated by the intermolecular contacts between the neighbor molecules in the first and second (111) surface molecular layers. Therefore, either the relaxation is spread over several layers or the molecular spheres themselves should be noticeably deformed. The elastic properties of ferritin molecules have not been tested. However, from the practice of handling of these crystals their hardness seem to be comparable with that of lysozyme.

The macroscopic scale surface roughness of about two to three molecular diameters seems to be reasonable since, according to AFM data, ferritin grows by two-dimensional nucleation and never shows spiral growth, and thus there are no vicinal hillocks that may result in larger scale roughness.

In summary, a 4% inward relaxation has been detected for the {111} face of ferritin crystals in aqueous solution. This implies a rearrangement of the molecular contact between the first and second layers, presumably due to the state of hydration. It is planned to measure the response of the relaxation to changes in the solvent composition in future experiments.

[1] A. McPherson, *Crystallization of Biological Macromolecules* (Cold Spring Harbor Laboratory Press, Cold Spring Harbor,

NY, 1999).

[2] P.H. Duke, *Synchrotron Radiation; Production and Properties*

(Oxford University Press, Oxford, 2000).

[3] J. Als-Nielsen and D. McMorrow, *Elements of Modern X-Ray Physics* (Wiley, West Sussex, 2001).

[4] A.A. Chernov, *Modern Crystallography III* (Springer-Verlag, Heidelberg, 1984).

[5] A.A. Chernov, Phys. Rep. **288**, 61 (1997).

[6] P.G. Vekilov, Prog. Cryst. Growth Charact. Mater. **26**, 25 (1993).

[7] Y.G. Kuznetov, A.J. Malkin, A. Geenwood, and A. McPherson, J. Struct. Biol. **114**, 184 (1995).

[8] Y.G. Kuznetsov, A.J. Malkin, and A. McPherson, J. Cryst. Growth **196**, 489 (1999).

[9] A.J. Malkin, T.A. Land, Y.G. Kuznetsov, A. McPherson, and J.J. DeYoreo, Phys. Rev. Lett. **75**, 2778 (1995).

[10] T.A. Land, J.J. DeYoreo, and J.D. Lee, Surf. Sci. **384**, 136 (1997).

[11] S.-T. Yau, D.N. Petsev, B.R. Thomas, and P.G. Vekilov, J. Mol. Biol. **303**, 667 (2000).

[12] S.-T. Yau, B.R. Thomas, and P.G. Vekilov, Phys. Rev. Lett. **85**, 353 (2000).

[13] N. Gvozdev, L. Rashkovich, and I. Yaminsky, in *Macromolecular Symposia*, edited by A.R. Khokhlov, Q. Tran-Cong-Miyata, V.A. Davidov, T. Yamaguchi, and S.I. Kuchanov (Wiley-VCH Verlag, Weinheim, Germany, 2000), Vol. 160, pp. 49–53.

[14] H. Li, M.A. Perozzo, J.H. Konnert, A. Nadarajah, and M.L. Pusey, Acta Crystallogr., Sect. D: Biol. Crystallogr. **55**, 1023 (1999).

[15] B.R. Thomas, D. Carter, and F. Rosenberger, J. Cryst. Growth **187**, 499 (1998).

[16] B.R. Thomas, A.A. Chernov, P. Vekilov, and D.C. Carter, J. Cryst. Growth **211**, 149 (2000).

[17] D.C. Carter, B. Wright, T. Miller, J. Chapman, P. Twigg, K. Keeling, K. Moody, M. White, J. Click, J.R. Ruble, J.X. Ho, L. Adcock-Downey, G. Bunick, and J. Harp, J. Cryst. Growth **196**, 602 (1999).

[18] P.M. Harrison and P. Arosio, Biochim. Biophys. Acta **1275**, 161 (1996).

[19] I.K. Robinson, H. Graafsma, K. Kvick, and J. Linderholm, Rev. Sci. Instrum. **66**, 1765 (1995).

[20] I.K. Robinson, Phys. Rev. B **33**, 3830 (1986).

[21] D. Schwarzenbach, *Crystallography* (Wiley, New York, 1996).

[22] D.A. Walko, Ph.D. thesis, University of Illinois, 2000.

[23] G.A. Somorjai and M.A. Van Hove, Prog. Surf. Sci. **30**, 201 (1989).

[24] K. Gekko, in *Water Relationships in Food*, edited by H. Levine and L. Slade (Plenum Press, New York, 1991), pp. 753–771.

[25] V.N. Morozov and T.Y. Morozova, Biopolymers **20**, 451 (1981).

[26] V.N. Morozov, T.Y. Morozova, E.G. Myachin, and G.S. Kachalova, Acta Crystallogr., Sect. B: Struct. Sci. **41**, 202 (1985).

[27] A.M. Holmes, W. K. Witherow, and A.A. Chernov (unpublished).

[28] J. Israelachvili, *Intermolecular and Surface Forces* (Academic Press, London, 1992), p. 124.